Nanoscale

Effect of pore density on gas permeation through nanoporous graphene membranes

Journal:	*Nanoscale*
Manuscript ID	NR-ART-03-2018-002625.R3
Article Type:	Paper
Date Submitted by the Author:	17-Jul-2018
Complete List of Authors:	Wang, Song; University of California, Riverside, Department of Chemistry Tian, Ziqi; Institute of Materials Technology and Engineering, Chinese Academy of Sciences Dai, Sheng; Oak Ridge National Laboratory, Jiang, De-en; University of California, Riverside, Department of Chemistry

SCHOLARONE™
Manuscripts

Effect of pore density on gas permeation through nanoporous graphene membranes

Song Wang,[a] Ziqi Tian,[b] Sheng Dai,[c,d] and De-en Jiang*,[a]

[a]Department of Chemistry, University of California, Riverside, California 92521, United States
[b]Ningbo Institute of Materials Technology and Engineering, Chinese Academy of Sciences, Ningbo, 315201, China
[c]Chemical Sciences Division, Oak Ridge National Laboratory, Oak Ridge, Tennessee 37831, United States
[d]Department of Chemistry, The University of Tennessee, Knoxville, Tennessee 37996, United States

ABSTRACT: Pore density is an important factor dictating gas separations through one-atom-thin nanoporous membranes, but how it influences the gas permeation is not fully understood. Here we use molecular dynamics (MD) simulations to investigate gas permeation through nanoporous graphene membranes with the same pore (3.0 Å × 3.8 Å in dimensions) but varying pore densities (from 0.01 to 1.28 nm^{-2}). We find that higher pore density leads to higher permeation per unit area of membrane for both CO_2 and He, but the rate of the increase decreases greatly for CO_2 at high pore densities. As a result, the per-pore permeance decreases for CO_2 but remains relatively constant for He with the pore density, leading to a dramatic change in CO_2/He selectivity. By separating the total flux into direct flux and surface flux, we find that He permeation is dominated by direct flux and hence the per-pore permeation rate is roughly constant with the pore density. In contrast, CO_2 permeation is dominated by surface flux and the overall decreasing trend of the per-pore permeation rate of CO_2 with the pore density can be explained by the decreasing per-pore coverage of CO_2 on the feed side with the pore density. Our work now provides a complete picture of the pore-density dependence of gas permeation through one-atom-thin nanoporous membranes.

1. INTRODUCTION

Graphene with subnanometer pores is promising as a one-atom-thin membrane for applications in separations of gases, water, ions, and isotopes.[1-11] Porous graphene was first proposed as the ultimate membrane for gas separation in 2009 by a computational proof-of-concept.[12] In 2012, molecular sieving of gases through porous graphene membranes with controlled pore sizes was experimentally demonstrated.[13] Meanwhile, porous graphene membranes and their derivatives have been predicted to be able to separate hydrogen isotopes.[14] To achieve scalable production of porous graphene membranes, graphene-oxide (GO) membranes have been fabricated and tested for gas separations.[15-17] Recently, other two-dimensional materials have also been examined as porous membranes.[18-23] For example, the MoS_2 nanosheets with suitable triangular pores were proposed for separating H_2 from N_2, CO, and CH_4 and for removing CO_2 from natural gas,[19] while molecular sieving of gases was shown for a MXene membrane.[23]

Although molecular sieving has been the main working mechanism for selective gas separations by porous graphene and related ultrathin membranes,[24] Drahushuk and Strano proposed two pathways of gas permeation through nanoporous graphene membranes from a detailed kinetic analysis: direct gas-phase pathway and adsorbed phase pathway.[25] In the gas-phase pathway, the flux scales with the pore area and the differential pressure. In the adsorbed phase pathway, the permeation is divided into five steps: adsorption, association, translocation, dissociation, and desorption.[25] Hadjiconstantinou et al. further explored the impact of pore size and pore functionalization on gas permeation through nanoporous graphenes by theoretical analysis and MD simulations.[26]

Although the role of pore density has been alluded to in several previous studies,[27-31] how exactly the pore density affects permeation has not been fully addressed, especially in the light of the direct gas-phase pathway vs the indirect adsorbed phase or surface pathway. In a more recent theoretical analysis combined with simulations for the adsorption-translocation mechanism, a minimum pore density has been identified for the porous graphene membrane to exceed the permeance-selectivity upper bound.[31] But a complete picture of the pore-density dependence of permeance would help guide both the top-down and bottom-up syntheses of ultrathin membranes of desired pore densities.

The goal of the present work is to understand the role of pore density in gas permeation through porous graphene. To this end, we have built a series of nanoporous graphene membrane models with different pore densities using the same pore, and then used classical molecular dynamics simulation to study the relationship of gas permeation with the pore density. We chose CO_2 and He, which represent two different types of gas molecule with strong and weak adsorption onto the nanoporous graphene membrane surface, respectively. By comparing the permeation behaviors of CO_2 and He, we aim to achieve a deeper understanding of how gas permeation depends on pore density on a porous graphene and to probe the direct vs indirect pathways.

2. COMPUTATIONAL METHOD

To simulate the effect of pore density, the same membrane dimensions of 10 nm × 10 nm and the same pore are employed, while the number of pores increases from 1 to 128 (Fig. 1a-h), corresponding to pore densities from 0.01 nm^{-2} to 1.28 nm^{-2}. The size of the simulation box is 10 nm × 10 nm × 20 nm. The pore has dimensions of 3.0 Å × 3.8 Å (see Fig. S1 in the electronic

supplementary information, ESI) and has been used previously for $H_2/CO_2/N_2/CH_4$ separations; it has very good performances for selective gas separations, for example, a selectivity of 300 for CO_2/N_2 separation with a CO_2 permeance on the order of 10^5 GPU.[32, 33] A bi-chamber system (Fig. 1i) with two-dimensional periodic boundary conditions is set up in our classical MD simulations, with the porous graphene membrane in the middle. The upper chamber is pressurized at 20 atm by 550 gas molecules of CO_2 or He for all graphene sheets of different pore densities, while the lower chamber is vacuum initially. MD simulations are performed using the LAMMPS package[34] in the canonical (NVT) ensemble at 300 K controlled using the Nose-Hoover thermostat.[35, 36] The force-field parameters for the membrane and gas molecules are taken from previous studies.[33, 37, 38] Only the non-bonded interactions (van der Waals and electrostatic) are considered. The graphene membrane is fixed and the gas molecules are rigid during the simulations. The Lennard-Jones parameters and partial atomic charges are provided in ESI. The cutoff distance for Lennard-Jones and Coulombic interactions is 12 Å; the long-range electrostatic interaction is calculated using the PPPM method.[39-41]

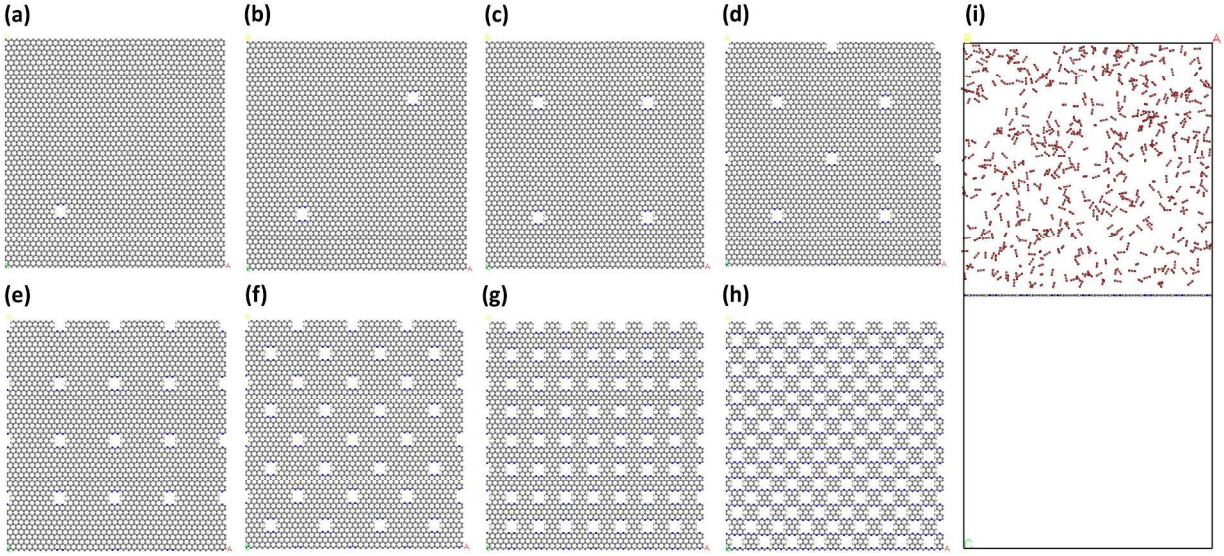

Fig. 1. The 10×10 nm^2 porous-graphene membrane with different pore densities of the same pore (3.0 Å ×3.8 Å in size; see Fig. S1 in ESI for a close-up view of the pore): (a) 0.01 nm^{-2}; (b) 0.02 nm^{-2}; (c) 0.04 nm^{-2}; (d) 0.08 nm^{-2}; (e) 0.16 nm^{-2}; (f) 0.32 nm^{-2}; (g) 0.64 nm^{-2}; (h) 1.28 nm^{-2}. (i) Side view of the bi-chamber setup for simulating gas permeation through the membrane in the middle; the upper chamber (the feed side) is pressurized at 20 atm while the lower chamber (the permeate side) is vacuum initially.

3. RESULTS AND DISCUSSION

3.1. Gas permeation through the nanoporous graphene membranes

Fig. 2 shows the MD simulation results of the number of the gas molecules permeating through the porous graphene membrane with time for different pore densities. One can see that for both CO_2 (Fig. 2a) and He (Fig. 2b), the permeation rate (the slope of the line) increases with the pore density. This can be more clearly seen in the first 5 ns of the simulations (Fig. 2c,d). In addition, one can see that when the pore density is relatively high (> 0.16 nm^{-2}), equilibrium can be reached within about 5 ns when pressure difference across the membrane approaches zero. To compare the permeation rates for the different pore densities, we used the initial slopes from our simulations (dashed lines in Fig. 2c,d).

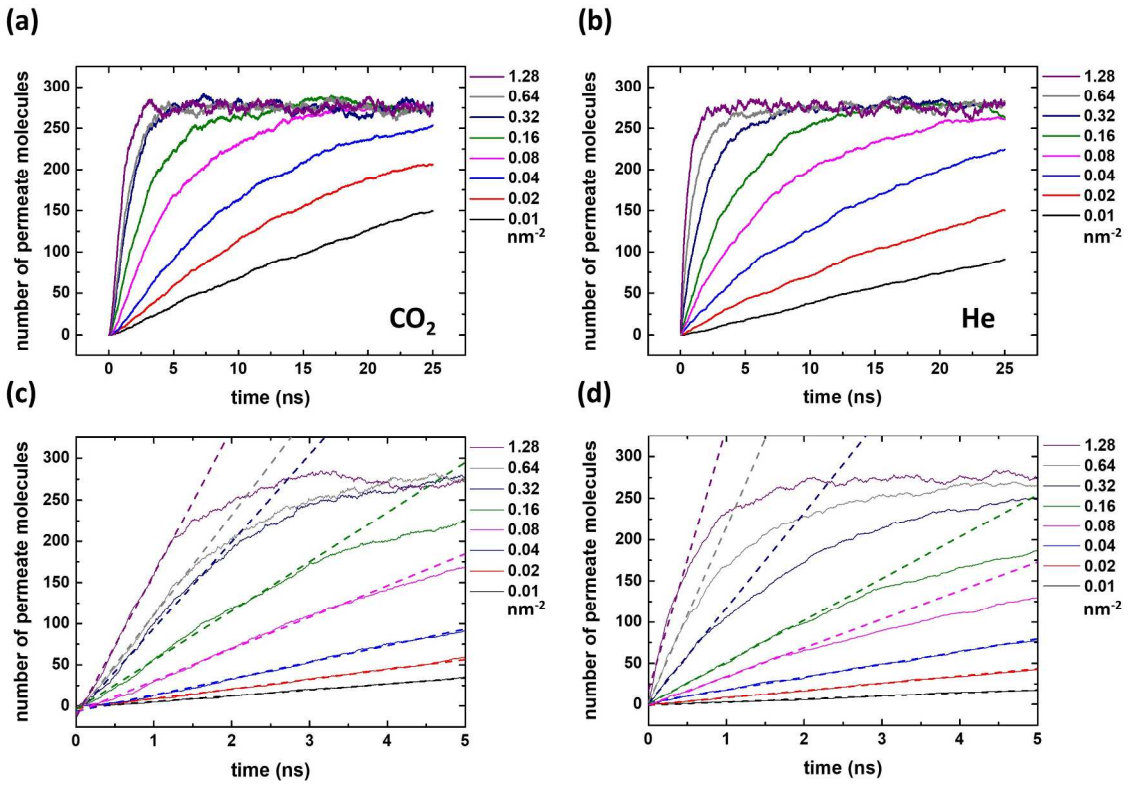

Fig. 2. The number of gas molecules permeating through the nanoporous graphene membrane with time for different pore densities (from 0.01 to 1.28 nm^{-2}): (a) CO_2 in 25 ns; (b) He in 25 ns; (c) CO_2 in 5 ns; (d) He in 5 ns. Dashed lines in (c) and (d) denote the permeation rates used to compute the initial fluxes.

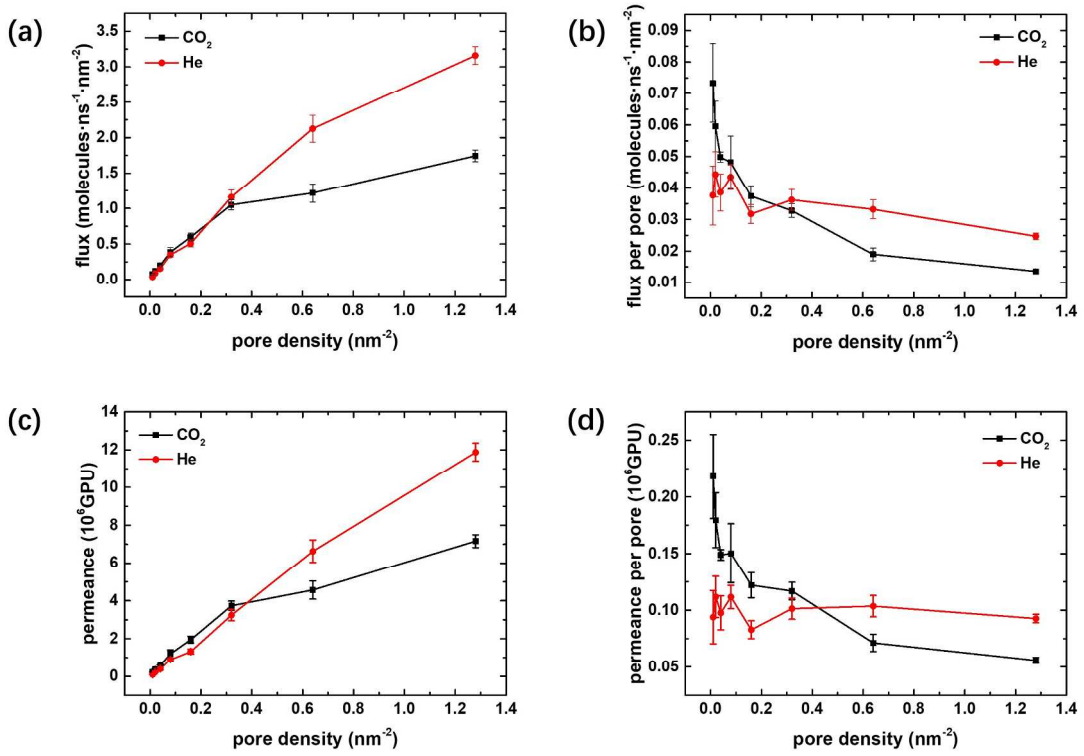

Fig. 3. Initial flux and permeance vs pore density of graphene membranes for CO_2 and He permeation: (a) flux per unit membrane area; (b) flux per pore; (c) permeance; (d) permeance per pore. Error bars are one standard deviation from averaging 10 parallel simulations.

From the initial permeation rate and the membrane total area (100 nm^2), we computed the initial flux as a function of the pore density. As shown in Fig. 3a, the flux of He increases almost linearly with the pore density, while the flux of CO_2 shows a similar linear increase when the pore density is < 0.3 nm^{-2} but the increase greatly slows down after 0.3 nm^{-2}. Since the pressure driving force changes with time differently for the different pore densities, we chose the 1-ns time point (that is, the time used to evaluate the initial fluxes) to evaluate the feed side and permeate side pressures as well as their difference (see Fig. S3 in ESI). Fig. 3c shows the pressure-normalized flux (that is, permeance), which displays a similar trend to the flux (Fig. 3a). At the pore density of 1.28 nm^{-2}, the flux of CO_2 is about 60% that of He and corresponds to a

permeance of ~ 6×10^6 GPU. This permeance is higher than the typical permeance found for one-atom-thin membranes (~ 10^4 to 10^5 GPU) from previous simulations[18, 33, 42, 43] because of the higher pore densities employed in this work. We also used an exponential decay model to fit the whole curves in Fig. 2 and obtained similar trends of fluxes for both CO_2 and He (see Fig. S3 in ESI).

The difference between CO_2 and He regarding the flux vs pore density trend can be more clearly seen in terms of the per-pore flux. One can see from Fig. 3b that at low pore densities the initial flux per pore is higher for CO_2 than He, even though He is smaller in size. This reverse selectivity is not uncommon in the literature of gas-separation membranes. For example, some polymeric membranes are selective for CO_2 than for the smaller H_2, due to CO_2's higher solubility in these polymers.[44] The underlying reason is similar in our case, due to the much more favorable surface adsorption of CO_2 than He on the membrane, as explained below. The dramatic change of the CO_2/He selectivity with the pore density is an interesting and major finding of the present work for the graphene membrane, which may have implications for designing reverse-selective membranes.

Over the whole range of the pore densities, Fig. 3b shows that the initial flux per pore is nearly constant for He, but displays a roughly exponential decay with the pore density for CO_2. This distinct and interesting difference between CO_2 and He begs a detailed analysis of their permeation behaviors through the porous graphene membranes of different pore densities. We first examine the adsorption behavior.

3.2. Gas adsorption on the nanoporous graphene membranes

Being a larger molecule with a large quadrupole moment, CO_2 adsorbs more strongly than He on the graphene membrane. Fig. 4 shows the distribution of CO_2 molecules along the direction perpendicular to the membrane surface after the equilibrium has been reached across the membrane. One can clearly see the adsorption layer on both sides of the membrane: each layer is about 5 Å thick, with the majority of the CO_2 molecules about 3 to 4 Å away from the graphene surface. Some CO_2 molecules with $z < 3$ Å are actually close to or in the pore.

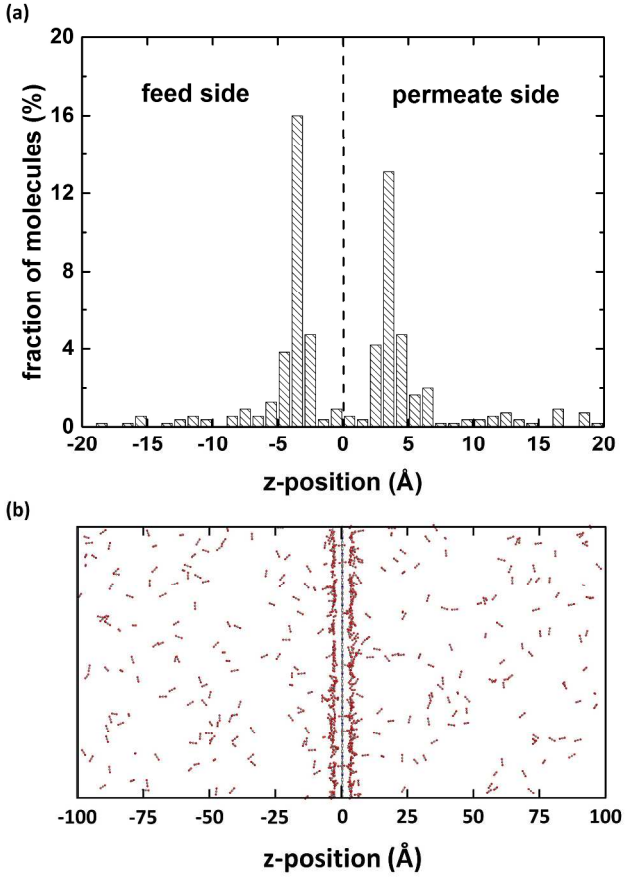

Fig. 4. CO_2 distribution along the z direction for a graphene membrane (at z=0) with the pore density of 1.28 nm^{-2} after 25 ns MD simulation: (a) statistical distribution at the 25-ns time point (bin size: 1 Å); (b) snapshot of CO_2 distribution at the 25-ns time point.

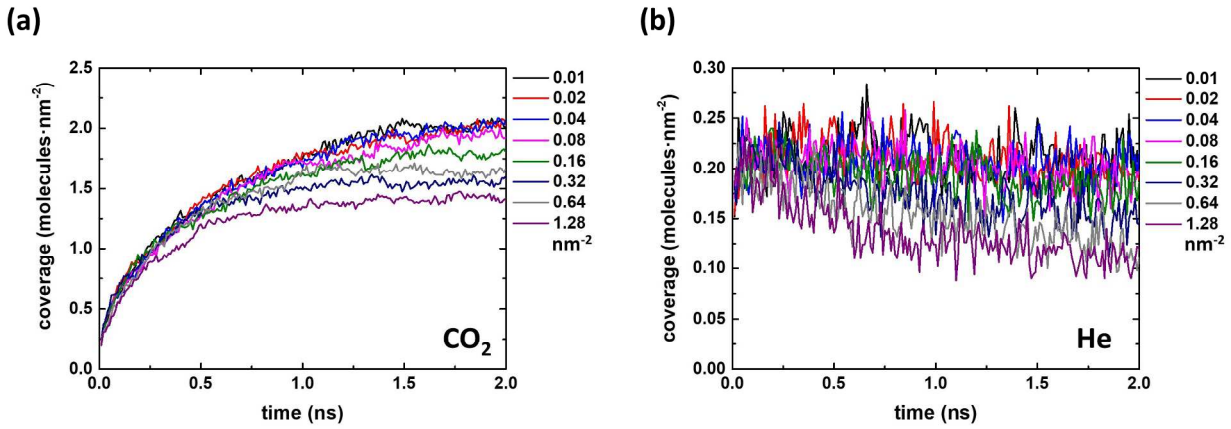

Fig. 5. Coverage of the gas adsorbate vs time on the feed side of the graphene membranes of different pore densities: (a) CO_2; (b) He.

Next we examine how fast the adsorption layers are built up on both sides of the graphene membrane. Fig. 5 shows the adsorption on the feed side of the membrane. One can see that regardless of the pore density, CO_2 adsorption on the feed side quickly reaches equilibrium within about 1 ns (Fig. 5a). In contrast, He coverage is much lower and shows much greater fluctuation (Fig. 5b). Similarly, we proceed to analyze the adsorption on the permeate or back side of the membrane. As shown in Fig. 6, the change of gas coverage with time displays a strong dependence on the pore density, especially for CO_2 (Fig. 6a). Fig. 7a shows that the initial adsorption rate on the permeate side increases with the pore density for both CO_2 and He. This increase is expected to closely correlate with the pressure rise in the permeate side; indeed, after pressure normalization, the adsorption rate becomes roughly constant at high pore densities (Fig. 7b).

Figs. 5-7 indicate that adsorption plays an important role in the dependence of CO_2 permeation on the pore density. However, to fully understand the trends in Fig. 3, we need to quantify the contribution of surface adsorption to the total flux relative to that of the direct flux.

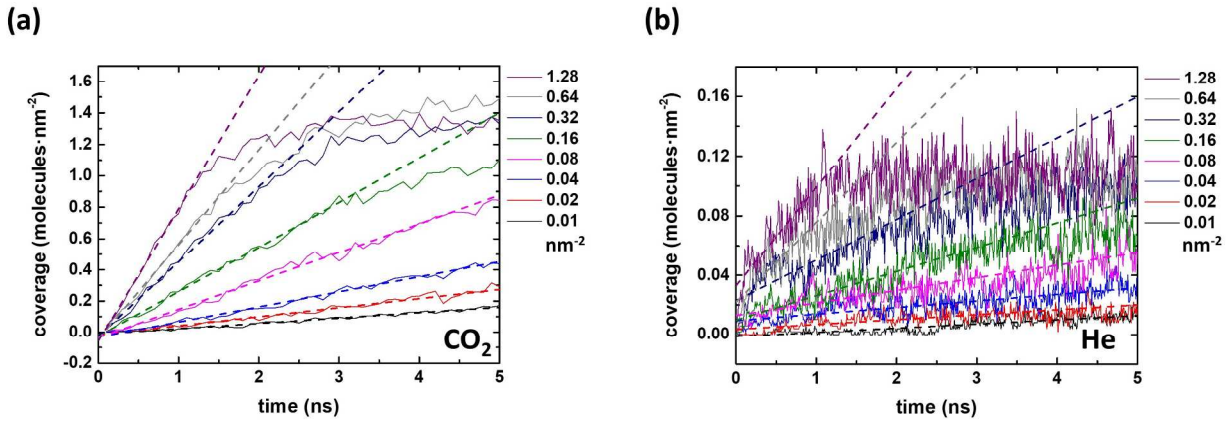

Fig. 6. Coverage of the adsorbate vs time on the permeate side of the graphene membrane of different pore densities: (a) CO_2; (b) He.

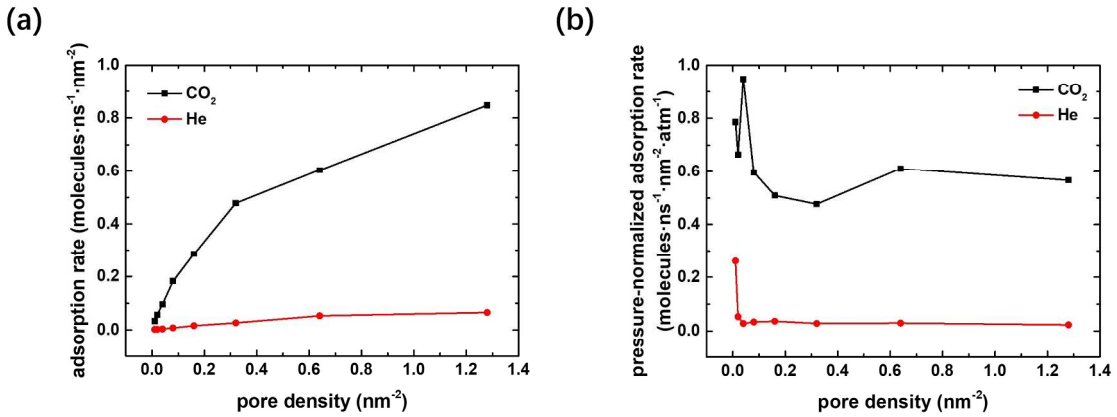

Fig. 7. (a) Adsorption rate and (b) pressure-normalized adsorption rate on the permeate side vs the pore density for CO_2 and He.

3.3. Surface flux vs direct flux

According to a previous kinetic analysis of gas permeation through a porous graphene membrane, the total flux can be decomposed into direct flux and surface flux.[25, 26] To assess their contributions, we have tracked all gas molecules in our simulations individually and analyzed their trajectories during the initial 1 ns, to determine the numbers of the different events. This allowed us to obtain the surface vs direct flux contributions. For He, we found that the total flux

is dominated by the direct flux, especially at high pore densities (see Fig. S4), due to weak adsorption (as evidenced from Fig. 5b and Fig. 6b). Since the direct flux scales with the permeable area (which in turn scales with the pore density), one expects a net flux linear with the pore density or a constant per-pore flux, as seen in Fig. 3 for He.

CO_2, on the other hand, shows a completely different behavior. We found that the CO_2 total flux per pore is dominated by the surface flux, as the direct flux is minor for all pore densities (Fig. 8), due to strong adsorption (as evidenced from Fig. 5a and Fig. 6a). Since the surface flux is relevant to surface adsorption, we will discuss the effect of adsorption behavior below.

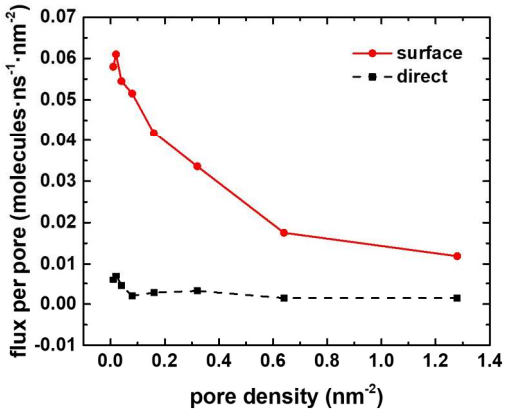

Fig. 8. The surface flux and the direct flux of CO_2, across graphene membranes of different pore densities. The values are from the trajectory analysis of all gas molecules during the initial 1 ns at 10 ps intervals. Molecules have to be adsorbed for 10 ps before crossing the membrane to be counted as the surface flux; molecules are counted as adsorbed if they are within 5 Å of the graphene membrane, even if they are over the pore; if a molecule crosses and then crosses back shortly after, we count it as zero.

3.4. The relationship between adsorption and surface flux for CO_2

As shown in Fig. S2a for CO_2, during the initial timeframe (within 1 ns) used for our flux analysis, the permeation is driven by the pressure difference across the graphene membrane and

the permeate-side pressure is much smaller than the feed-side pressure. Indeed, Fig. 9 shows that the per-pore coverage on the feed side is much greater than on the permeate side. Since surface flux is the dominating path for CO_2 permeation (Fig. 8) which is then dictated by the feed-side adsorption, the decreasing trend of the per-pore coverage of CO_2 on the feed side can well explain the decreasing per-pore flux of CO_2 with the pore density (Fig. 3b). In other words, as the pore density increases, the number of adsorbed molecules (on the feed side) available to each pore decreases, leading to a decreasing flux.

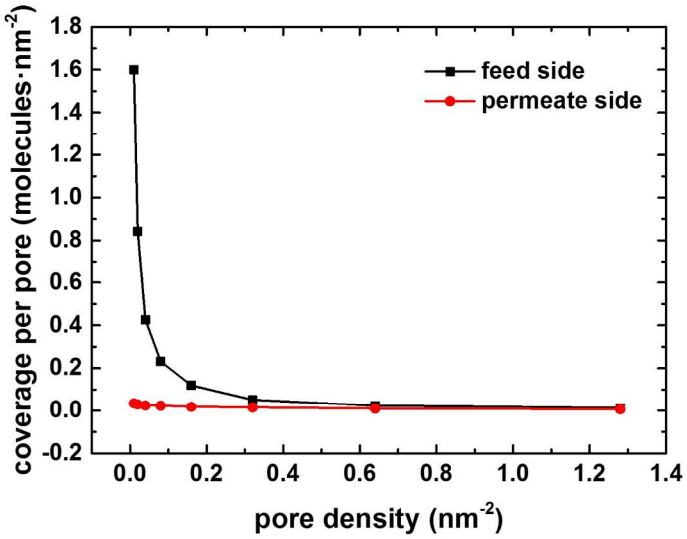

Fig. 9. Per-pore coverage of CO_2 on feed and permeate sides of the graphene membrane at different pore densities. Coverage data are at 1 ns.

3.5. Implications

The present work revealed some interesting trends of gas permeation across the porous graphene membranes of different pore densities. Our simulations showed that the higher the pore density, the greater the flux for both strongly and weakly adsorbing gases. More important, we found that the adsorption on both sides of the membrane greatly modulates the dependence of the flux on the pore density for a strongly adsorbing gas such as CO_2. The observation suggests that

making the membranes asymmetric by creating dissimilar surfaces could lead to more interesting permeation behavior.

Our models of the porous graphene with the high pore densities of the same pore can be best realized via the bottom-up chemical approach toward the two-dimensional covalent frameworks. A recent report just demonstrated this approach experimentally.[45] In the case of the top-down approach to creating pores in graphene, a distribution of the pore sizes is most likely. In this case, the effect of the pore density is complicated by the pore size distribution; previous analysis showed that gas permeation will be dominated by the larger pore if its concentration is significant.[12]

4. CONCLUSIONS

We have investigated permeation of CO_2 and He through nanoporous graphene membranes with varying pore densities (from 0.01 nm^{-2} to 1.28 nm^{-2}) by using molecular dynamics (MD) simulations. Higher pore density was found to yield higher permeation rate for both CO_2 and He per unit area of membrane, but the increase slows down greatly for CO_2. Separating the total permeation flux into direct flux and surface flux allowed us to find that He permeation is dominated by direct flux, leading to a relatively flat per-pore flux with the pore density. In contrast, CO_2 permeation is dominated by the surface flux. The per-pore flux of CO_2 decreases with the pore density overall, mainly due to the decreasing per-pore coverage of the adsorbed CO_2 molecules on the feed side. The present work provides insights into the pore-density dependence of gas permeation through a one-atom-thin membrane and also suggests new ways to improve the design of ultrathin membranes for gas separations.

Electronic supplementary information (ESI) available: atomic structure of the pore; force field parameters; exponential fitting model; pressures across the membrane at different pore densities; flux analysis for He molecule.

Conflicts of interest

There are no conflicts to declare.

Acknowledgements

This work was supported by the Division of Chemical Sciences, Geosciences and Biosciences, Office of Basic Energy Sciences, U.S. Department of Energy. This research used resources of the National Energy Research Scientific Computing Center, a DOE Office of Science User Facility supported by the Office of Science of the U.S. Department of Energy under Contract No. DE-AC02-05CH11231.

References

1 Z. Q. Tian, S. Dai and D. E. Jiang, *WIREs Comput. Mol. Sci.*, 2016, **6**, 173-197.

2 S. Gadipelli and Z. X. Guo, *Prog. Mater. Sci.*, 2015, **69**, 1-60.

3 S. P. Surwade, S. N. Smirnov, I. V. Vlassiouk, R. R. Unocic, G. M. Veith, S. Dai and S. M. Mahurin, *Nat. Nanotechnol.*, 2015, **10**, 459-464.

4 G. P. Liu, W. Q. Jin and N. P. Xu, *Chem. Soc. Rev.*, 2015, **44**, 5016-5030.

5 M. E. Suk and N. R. Aluru, *J. Phys. Chem. Lett.*, 2010, **1**, 1590-1594.

6 D. Cohen-Tanugi and J. C. Grossman, *Nano Lett.*, 2012, **12**, 3602-3608.

7 K. Sint, B. Wang and P. Kral, *J. Am. Chem. Soc.*, 2008, **130**, 16448-16449.

8 G. H. Hu, M. Mao and S. Ghosal, *Nanotechnology*, 2012, **23**, 395501.

9 A. P. Ji, Z. W. Li, H. J. Yang, P. Y. He and Y. F. Chen, *Biophys. J.*, 2017, **112**, 544a.

10 A. W. Hauser and P. Schwerdtfeger, *J. Phys. Chem. Lett.*, 2012, **3**, 209-213.

11 A. W. Hauser, J. Schrier and P. Schwerdtfeger, *J. Phys. Chem. C*, 2012, **116**, 10819-10827.

12 D. E. Jiang, V. R. Cooper and S. Dai, *Nano Lett.*, 2009, **9**, 4019-4024.

13 S. P. Koenig, L. D. Wang, J. Pellegrino and J. S. Bunch, *Nat. Nanotechnol.*, 2012, **7**, 728-732.

14 M. Hankel, Y. Jiao, A. J. Du, S. K. Gray and S. C. Smith, *J. Phys. Chem. C*, 2012, **116**, 6672-6676.

15 H. Li, Z. N. Song, X. J. Zhang, Y. Huang, S. G. Li, Y. T. Mao, H. J. Ploehn, Y. Bao and M. Yu, *Science*, 2013, **342**, 95-98.

16 H. W. Kim, H. W. Yoon, S. M. Yoon, B. M. Yoo, B. K. Ahn, Y. H. Cho, H. J. Shin, H. Yang, U. Paik, S. Kwon, J. Y. Choi and H. B. Park, *Science*, 2013, **342**, 91-95.

17 B. X. Mi, *Science*, 2014, **343**, 740-742.

18 Z. Q. Tian, S. Dai and D. E. Jiang, *ACS Appl. Mater. Inter.*, 2015, **7**, 13073-13079.

19 Y. D. Zhang, Z. S. Meng, Q. Shi, H. Q. Gao, Y. Z. Liu, Y. H. Wang, D. W. Rao, K. M. Deng and R. F. Lu, *J. Phys. Condens. Mat.*, 2017, **29**, 375201.

20 B. Xu, H. Xiang, Q. Wei, J. Q. Liu, Y. D. Xia, J. Yin and Z. G. Liu, *Phys. Chem. Chem. Phys.*, 2015, **17**, 15115-15118.

21 G. P. Liu, W. Q. Jin and N. P. Xu, *Angew. Chem. Int. Ed.*, 2016, **55**, 13384-13397.

22 Z. K. Zheng, R. Grunker and X. L. Feng, *Adv. Mater.*, 2016, **28**, 6529-6545.

23 L. Ding, Y. Y. Wei, L. B. Li, T. Zhang, H. H. Wang, J. Xue, L. X. Ding, S. Q. Wang, J. Caro and Y. Gogotsi, *Nat. Commun.*, 2018, **9**, 155.

24 A. F. Ismail and L. I. B. David, *J. Membrane Sci.*, 2001, **193**, 1-18.

25 L. W. Drahushuk and M. S. Strano, *Langmuir*, 2012, **28**, 16671-16678.

26 C. Z. Sun, M. S. H. Boutilier, H. Au, P. Poesio, B. F. Bai, R. Karnik and N. G. Hadjiconstantinou, *Langmuir*, 2014, **30**, 675-682.

27 J. K. Holt, H. G. Park, Y. M. Wang, M. Stadermann, A. B. Artyukhin, C. P. Grigoropoulos, A. Noy and O. Bakajin, *Science*, 2006, **312**, 1034-1037.

28 S. Sircar, T. C. Golden and M. B. Rao, *Carbon*, 1996, **34**, 1-12.

29 D. L. Gin and R. D. Noble, *Science*, 2011, **332**, 674-676.

30 H. J. Liu, S. Dai and D. E. Jiang, *Solid State Commun.*, 2013, **175**, 101-105.

31 Z. Yuan, A. G. Rajan, R. P. Misra, L. W. Drahushuk, K. V. Agrawal, M. S. Strano and D. Blankschtein, *ACS Nano*, 2017, **11**, 7974-7987.

32 H. J. Liu, Z. F. Chen, S. Dai and D. E. Jiang, *J. Solid State Chem.*, 2015, **224**, 2-6.

33 H. J. Liu, S. Dai and D. E. Jiang, *Nanoscale*, 2013, **5**, 9984-9987.

34 S. Plimpton, *J. Comput. Phys.*, 1995, **117**, 1-19.

35 S. Nose, *J. Chem. Phys.*, 1984, **81**, 511-519.

36 W. G. Hoover, *Phys. Rev. A*, 1985, **31**, 1695-1697.

37 S. Neyertz, *Macromol. Theory Simul.*, 2007, **16**, 513-524.

38 R. A. Aziz, A. R. Janzen and M. R. Moldover, *Phys. Rev. Lett.*, 1995, **74**, 1586-1589.

39 R. W. Hockney and J. W. Eastwood, *Computer simulation using particles*, CRC Press, 1988.

40 I. C. Yeh and M. L. Berkowitz, *J. Chem. Phys.*, 1999, **111**, 3155-3162.

41 V. Ballenegger, A. Arnold and J. J. Cerda, *J. Chem. Phys.*, 2009, **131**, 094107.

42 J. Schrier, *ACS Appl. Mater. Inter.*, 2012, **4**, 3745-3752.

43 M. S. Strano and H. C. Foley, *Carbon*, 2002, **40**, 1029-1041.

44 H. Q. Lin, E. Van Wagner, B. D. Freeman, L. G. Toy and R. P. Gupta, *Science*, 2006, **311**, 639-642.

45. C. Moreno, M. Vilas-Varela, B. Kretz, A. Garcia-Lekue, M. V. Costache, M. Paradinas, M. Panighel, G. Ceballos, S. O. Valenzuela, D. Peña and A. Mugarza, *Science*, 2018, **360**, 199-203.

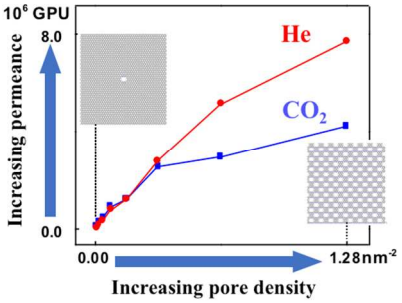

The pore-density dependence of gas permeation through one-atom-thin membranes displays different trends for different gases due to their different permeation-mechanisms.